Peaks and Distributions of White Matter Tract-related Strains in Bicycle Helmeted Impacts: Implication for Helmet Ranking and Optimization

Zhou Zhou,[1*] Madelen Fahlstedt,[2] Xiaogai Li,[1] Svein Kleiven[1]

[1] Neuronic Engineering, KTH Royal Institute of Technology, Stockholm, 14152, Sweden.

[2] Mips AB, Täby, Sweden.

[*] Corresponding author: Zhou Zhou Email: zhouz@kth.se

Email addresses of other authors:

Madelen Fahlstedt: madelen.fahlstedt@mipsprotection.com

Xiaogai Li: xiaogai@kth.se

Svein Kleiven: sveink@kth.se

Abstract

Traumatic brain injury (TBI) in cyclists is a growing public health problem, with helmets being the major protection gear. Finite element head models have been increasingly used to engineer safer helmets often by mitigating brain strain peaks. However, how different helmets alter the spatial distribution of brain strain remains largely unknown. Besides, existing research primarily used maximum principal strain (MPS) as the injury parameter, while white matter fiber tract-related strains, increasingly recognized as effective predictors for TBI, have rarely been used for helmet evaluation. To address these research gaps, we used an anatomically detailed head model with embedded fiber tracts to simulate fifty-one helmeted impacts, encompassing seventeen bicycle helmets under three impact conditions. We assessed the helmet performance based on four tract-related strains characterizing the normal and shear strain oriented along and perpendicular to the fiber tract, as well as the prevalently used MPS. Our results showed that both the helmet type and impact condition affected the strain peaks. Interestingly, we noted that helmets did not alter strain distribution, except for one helmet under one specific impact condition. Moreover, our analyses revealed that helmet ranking outcome based on strain peaks was affected by the choice of injury metrics (Kendall's tau coefficient: 0.58 ~ 0.93). Significant correlations were noted between tract-related strains and angular motion-based injury metrics. This study provided new insights into computational brain biomechanics and highlighted the helmet ranking outcome was dependent on the choice of injury metrics. Our results also hinted that the performance of helmets could be augmented by mitigating the strain peak and optimizing the strain distribution with accounting the selective vulnerability of brain subregions.

Keywords

Bicycle helmet, computational impact simulation, strain peak and distribution, injury metrics, helmet ranking and optimization

Introduction

Traumatic brain injury (TBI) in cyclists is a concerning public health problem worldwide. In the United States, the annual number of emergency department visits for nonfatal bicycle-related TBI was around 596,972, with a large proportion of survived cyclists experiencing neurocognitive and behavioural sequelae (Sarmiento 2021). In the Netherlands, the incidence of hospital admission due to bicycle-related TBI surged by 92% between 1998 and 2012, accompanied by an estimated annual economic cost of around 74.5 million Euros (Scholten *et al.* 2015). Injury data of cyclists in Sweden also showed that head injuries, in comparison to other trauma types, were more likely to cause permanent medical impairment (Rizzi *et al.* 2013). Given the increased popularity of bicycling as a recreational activity and transportation mode (Piatkowski and Bopp 2021), this TBI-related urgency in cyclists is expected to continuously grow and calls for effective prevention strategies (Næss *et al.* 2020).

Bicycle helmets are the most prevalent wearable gear for TBI prevention in cyclists by reducing the force acting on the head (Leng *et al.* 2022). Existing bicycle helmets are engineered with the primary goal of passing the certification standard for commercialization purposes. For example, in Europe, the bicycle helmet is tested by dropping a helmeted headform onto a flat surface or kerbstone (i.e., direct impact) with the resultant peak linear acceleration (PLA) below 250 g (EN 1078). Similar standards exist in other countries, e.g., CPSC 16 CFR Part 1203 in the United States, GB 24429 in China, AS/NZS 2063 in Australia and New Zealand, etc. A detailed comparison of different bicycle helmet test standards is available in several recent reviews (Whyte *et al.* 2019, Emsley *et al.* 2024). However, existing helmet testing standards all focused on direct impacts with pass/fail criteria based on linear motion-related metrics (e.g., PLA, Head Injury Criterion (HIC)). Considering the prevalence of oblique impacts in real-life bicycle accidents (Baker *et al.* 2023) and the primary role of angular motion in brain injury mechanics (King *et al.* 2003, Kleiven 2013), several consortiums, such as the CEN Technical Committee 158 Working Group 11 in Europe, strived to improve the test standard by involving oblique impact scenarios (e.g., collisions against an angled surface) and angular motion-related metrics (e.g., peak angular velocity (PAV)) as the pass/fail threshold (Halldin *et al.* 2001, Halldin *et al.* 2003), proposing multiple pilot bicycle helmet rating programmes (Mills and Gilchrist 2008, Dau *et al.* 2012, Hansen *et al.* 2013, Willinger *et al.* 2014, Klug *et al.* 2015, Stigson *et al.* 2017, Deck *et al.* 2019, Bland *et al.* 2020). However, there is no bicycle helmet testing standard with oblique impacts today.

Despite the progress in better reflecting the impact scenarios in bicycle accidents and brain injury mechanisms in the pilot rating programmes, one limitation is that the kinematic-based injury metrics (regardless of linear motion- or angular motion-based ones) are commonly used (Mills and Gilchrist 2008, Dau *et al.* 2012, Klug *et al.* 2015, Bland *et al.* 2020). Kinematic-based metrics only quantify the gross motion of the head and provide little information on how the brain and its subregions respond during helmeted impacts. To address this, researchers resort to finite element (FE) head models that can

offer spatiotemporal detailed information on intracranial responses to external impacts of any magnitude and direction. Once appropriately evaluated against cadaveric experiments and real-life TBI accidents, the FE head model is an invaluable tool to assess the efficacy of different countermeasures based on tissue-level injury metrics (e.g., stress and strain) that demonstrated superior injury predictability than kinematic-based injury metrics (Zhang *et al.* 2004, Kleiven 2007, Giordano and Kleiven 2014, Zhao *et al.* 2017, Wu *et al.* 2020, Wu *et al.* 2021, Wu *et al.* 2022, Meng *et al.* 2023). A growing body of literature has evaluated the performance of bicycle helmets with the aid of the FE model (Fahlstedt *et al.* 2014, Ito *et al.* 2014, Fahlstedt *et al.* 2016a, Pipkorn *et al.* 2020, Abayazid *et al.* 2021, Hoshizaki *et al.* 2022, Wang *et al.* 2023, Li *et al.* 2024). For example, Fahlstedt *et al.* (2016a) assessed the performance of one helmet in three accidental scenarios using the KTH Royal Institute of Technology head model and found that wearing a helmet reduced the maximum principal strain (MPS) in the brain by up to 45%. Abayazid *et al.* (2021) evaluated 27 bicycle helmets using another head model and found the performance of different protection technologies in terms of mitigating strain peaks was dependent on the impact direction. Several studies (Willinger *et al.* 2014, Stigson *et al.* 2017, Deck *et al.* 2019) proposed to integrate FE head models within the helmet rating programmes, although the capability of FE models for such a stringent application is at the forefront of the debate (Fahlstedt *et al.* 2021).

For brain responses during helmeted impacts, one fundamental question that is largely unknown is how different helmets alter the spatial distribution of tissue response. This is evidenced by the fact that the existing studies primarily focused on the peak value of tissue-based metrics, e.g., MPS (Fahlstedt *et al.* 2014, 2016a, Fahlstedt *et al.* 2016b, Stigson *et al.* 2017, Pipkorn *et al.* 2020, Abayazid *et al.* 2021, Hoshizaki *et al.* 2022, Meng *et al.* 2023, Abayazid and Ghajari 2024, Li *et al.* 2024), maximum shear strain (Ito *et al.* 2014), maximal strain rate (Abayazid *et al.* 2021), maximal von-Mises strain (Willinger *et al.* 2014), and maximal von-Mises stress (Deck *et al.* 2019). Complementary efforts were noted to quantify the volume fraction of brain element with the strain peak over a certain threshold (i.e., the cumulative strain damage measure (CSDM) (Bandak and Eppinger 1994)) in helmeted impacts, but CSDM still could not provide location information of these “high-strained” elements. Even beyond the context of helmeted impacts, we found that only a handful of studies used FE models to investigate brain strain distribution using either synthetic angular loadings scaled from laboratory reconstructed impacts (Zhao and Ji 2017) or idealized sinus-shaped angular impacts (Carlsen *et al.* 2021). Investigating the patterns of brain tissue responses in realistic helmeted impacts not only addresses an important research gap in brain biomechanics and may also provide new insights for helmet optimization.

Another important challenge when using the FE head model for helmet evaluation is how best to interpret the response of FE model. Today, no consensus has been reached on the optimal tissue-based metrics for brain trauma prediction, as is partially substantiated by the discordant choice described above. Recent studies from several independent groups reported that the normal strain oriented along the fiber tract (i.e., tract-oriented normal strain, alternatively termed as tract-oriented strain, axonal strain, or fiber

strain in the literature) demonstrated superior injury predictability than its counterparts (e.g., MPS) (Giordano and Kleiven 2014, Sahoo *et al.* 2016, Zhao *et al.* 2017, Hajiaghamemar *et al.* 2020b). In 2024, Zhou *et al.* (2024) presented a mathematical framework to comprehensively quantify the *in vivo* white matter (WM) tract-related deformation during voluntary impacts based on three new strain measures, characterizing the normal strain perpendicular to the fiber tract (i.e., tract-perpendicular normal strain) and shear strains oriented along and perpendicular to the fiber tract (i.e., tract-oriented shear strain, tract-perpendicular shear strain, respectively). This framework could be extended to *in silico* simulations to extract tract-related strains in helmeted impacts. This might be particularly important given the prevalence of axonal pathology in TBI accidents (Johnson *et al.* 2013, Song *et al.* 2022) and the great potential of tract-related strains for axonal injury prediction. When relating to helmet evaluation, one interesting question that can be asked is how close the newly proposed tract-related strains discriminate the helmet performance to the prevalently used MPS.

The current study aimed to answer how different helmets influence brain strain patterns and how the helmet ranking outcome was affected by the choice of tissue-based injury metric. To this end, we extracted experimental kinematics from fifty-one helmeted impacts, covering seventeen helmets and three impact conditions. These impact loadings were imposed to an anatomically detailed FE head model with embedded axonal fiber tracts to predict the distribution and peak of four tract-related strains and MPS. The helmet performance was ranked based on five strain peaks. This study provided new insights into computational brain biomechanics and virtual ranking of helmet efficacy. It might also serve as a reference for helmet improvement, especially those intended to optimize brain strain distribution.

Methods

Laboratory helmet tests

All experiments were performed by the Folksam Insurance Group and described with greater detail available elsewhere (Stigson *et al.* 2017). In brief, seventeen commercially available bicycle helmets were purchased online or in-store from the Swedish market and tested in the laboratory to obtain impact kinematics. These seventeen helmets (Helmets A-Q, Fig 1A) were selected with the intention to represent the commonly used ones featured with different designs and protection technologies. Each helmet was coupled with a 50th percentile male Hybrid III headform and dropped onto a 45˚ anvil (covered with abrasive paper, impact speed: 6 m/s) at three different impact conditions (Fig 1B, referred to as XRot, YRot, and ZRot hereafter), each of which was expected to cause rotational motion primarily within one anatomical plane. In total, fifty-one helmeted impact experiments were performed with the linear and angular accelerations at the center of gravity of the headform recorded.

To quantify the helmeted impact responses, seven kinematic-based metrics were computed. These include two linear motion-based metrics (i.e., PLA and HIC (Versace 1972)) and five angular motion-based metrics (i.e., peak angular acceleration (PAA), PAV (Kleiven 2006), Brain Injury Criterion (BrIC)

(Kleiven 2006, Takhounts *et al.* 2013), Universal Brain Injury Criterion (UBrIC) (Gabler *et al.* 2018), and Diffuse Axonal, Multi-Axis, General Evaluation (DAMAGE) (Gabler *et al.* 2019)). Equations for computing these metrics are summarized in Table 1A.

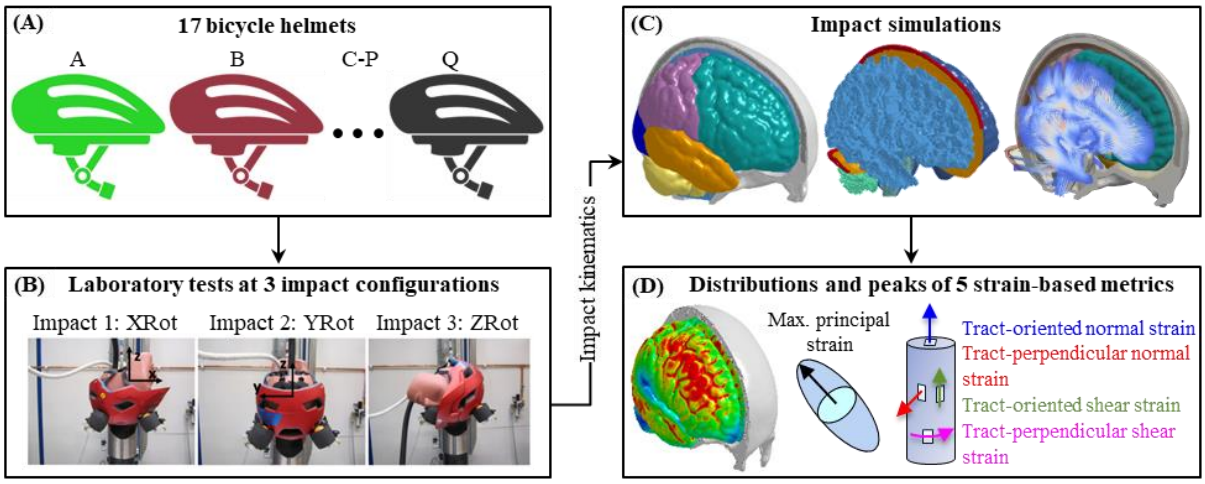

Fig. 1. Illustration of study design and methodology. Seventeen helmets (named as Helmet A to Helmet Q) (**A**) were tested in three impact scenarios (named as XRot for impact 1, YRot for impact 2, and ZRot for impact 3) (**B**). The recorded impact kinematics were imposed to a computational head model with embedded white matter fiber tracts (**C**) to compute the brain responses based on five strain-related metrics (**D**).

Helmeted impact simulations

To estimate the localized brain strain responses, the experimental kinematics from the helmeted laboratory tests were imposed to an anatomically detailed computational head model (i.e., the ADAPT model in Fig 1C). The ADAPT model was developed previously at KTH Royal Institute of Technology in Stockholm using the LS-DYNA software with details about geometrical discretization, material modelling, interfacial representation, and model validation available elsewhere (Li *et al.* 2021, Zhou *et al.* 2023). The model included gray matter, white matter (WM), cerebrospinal fluid, ventricles, skull, and meninges. To enable the calculation of tract-related deformation, the axonal fiber tract was embedded within the WM (Li *et al.* 2021, Zhou *et al.* 2022). Fifty-one impact simulations were performed, corresponding to the seventeen helmets tested in three impact conditions. To simulate the helmeted impacts, the directional linear acceleration and angular velocity curves (shown in Fig A1 in Appendix) were imposed to one node located at the head's centre of gravity and constrained to the rigidly modelled skull. All simulations lasted for 30 ms, starting from the instant the helmet made contact with the angled surface. The peak strain values of all elements were reached with the simulated impact duration.

To evaluate the brain responses in helmeted impact simulations, five strain-based metrics were employed (Fig 1D & Table 1B), including one brain tissue-level strain (i.e., MPS) and four WM tract-related strains (i.e., maximum tract-oriented normal strain (MTON), maximum tract-perpendicular normal strain (MTPN), maximum tract-oriented shear strain (MTOS), and maximum tract-perpendicular shear strain (MTPS)). The MPS was extracted for all brain elements (N = 513,198) and directly output from the simulation. The tract-related strains were only computed for WM elements (N = 213,321) with

the exact mathematical equations presented in our previous study (Zhou *et al.* 2024). The peak values accumulated over time were extracted for all strain-based metrics.

Table. 1. Seven kinematic-based metrics (A) and five strain-based metrics (B) used in this study. Note that the coordinate system (*xyz*) used to compute the kinematic-based metrics is the same as the one in Fig 1B.

(A)	Abbreviation & Equations	Notes
Kinematic-based metrics	PLA = max (a(t))	a(t) is the resultant linear acceleration
	$\mathrm{HIC} = \max\left\{(t_2 - t_1)\left(\frac{1}{t_2 - t_1}\int_{t_1}^{t_2} a(t)dt\right)^{2.5}\right\}$	a(t) is the resultant linear acceleration and t_2-t_1 represents a time interval of 15 ms.
	PAA = max (α (t))	α (t) is the resultant angular acceleration
	PAV = max (ω(t))	ω(t) is the resultant angular velocity
	$\mathrm{BrIC}=\sqrt{\left(\frac{\omega_x}{\omega_{xc}}\right)^2+\left(\frac{\omega_y}{\omega_{yc}}\right)^2+\left(\frac{\omega_z}{\omega_{zc}}\right)^2}$	ω_x, ω_y, and ω_z are the maximal angular velocities along *x*-, *y*-, and *z*-axes, respectively. ω_{xc}, ω_{yc}, and ω_{zc} are corresponding critical values (66.2, 59.1, and 44.2 rad/s).
	$\mathrm{UBrIC}=\left\{\sum_i\left[w_i^* + (\alpha_i^* - w_i^*)e^{-\frac{\alpha_i^*}{w_i^*}}\right]\right\}^r$ $w_i^* = w_i/w_{icr}$ and $\alpha_i^* = \alpha_i/\alpha_{icr}$	w_i and α_i (i =*x*, *y*, *z*) are the maximum angular velocity and angular acceleration along *x*-, *y*-, and *z*-axes. The resting are predefined values: w_{xcr}, w_{ycr}, and w_{zcr} are 211, 171, and 115 rad/s; α_{xcr}, α_{ycr}, and α_{zcr} are 20.0, 10.3, and 7.76 krad/s^2; r is 2.
	$\mathrm{DAMAGE} = \beta\max_t\{\lvert\bar{\delta}(t)\rvert\}$	β is a scalar factor set to 2.9903; $\bar{\delta}(t)$ is displacement time histories of the three coupled masses
(B)	Abbreviation	Description
Tissue-based metrics	MPS	The maximum value of the 1st principal Green-Lagrange strain in the brain across the simulation
	MTON	The maximum value of normal strain oriented along the white matter fiber tract across the simulation
	MTPN	The maximum value of peak normal strain perpendicular to the white matter fiber tract across the simulation
	MTOS	The maximum value of shear strain oriented along the white matter fiber tract across the simulation
	MTPS	The maximum value of peak shear strain perpendicular to the white matter fiber tract across the simulation

Data analyses

To quantify variations in peak strains among seventeen helmets, we calculated the 95th percentile value of MPS across the whole brain and four tract-related strain peaks across the WM for each impact simulation. To statistically ascertain the influence of impact conditions (XRot, YRot, and ZRot) on brain response, the peak strain results (non-normally distributed) were analysed with a Wilcoxon matched pairs signed rank test.

We ranked the seventeen helmets (Helmets A-Q) based on the strain peaks averaged across three impact conditions, the same approach as adopted by Fahlstedt *et al.* (2021). To assess the choice of strain-based metrics (five strains, Table 1B) on the helmet ranking outcome, Kendall's tau coefficients were calculated based on the ranking results (10 different combinations). Pearson's correlations were conducted to test the dependency between seven kinematic-based metrics and five strain-based metrics (35 tests), as well as among the five strain-based metrics themselves (10 tests).

To qualitatively visualize whether different helmets alter the strain distribution, we identified the elements with the strain value ranked within the top 5% across the whole brain for MPS and the whole WM for tract-related strains for each simulation. We also normalized the element-wise strain by the 95th percentile maximum strain result of the same simulation, similar to the approach of one early work

(Carlsen *et al.* 2021). To quantitatively assess the similarity of strain distributions in different helmeted impact simulations, Pearson's correlation was conducted between element-wise strain peaks from the same impact condition, akin to the method in one previous study (Zhao and Ji 2017). The current work involved seventeen helmets, three impact conditions and five strain-based metrics, resulting in a total of 2040 Pearson's correlation analyses (i.e., $C_{17}^{2} \times 3 \times 5$). The threshold for significance was set to $p < 0.05$. The correlation level was determined by the coefficient value (r) (i.e., 0 ~ 0.3 for weak correlation, 0.3 ~ 0.7 for moderate correlation, and 0.7 ~ 1 for strong correlation) (Ratner 2009).

Results

The current study focused on the helmet's influence on the brain strain peak and distribution. Helmeted impact kinematics have been reported earlier (Stigson *et al.* 2017, Fahlstedt *et al.* 2021) and were not reiterated herein. To ensure the completeness of our study, we only presented a summary of seven kinematic-based metrics in Fig 2A with the detailed acceleration and velocity curves for the fifty-one helmeted impacts available in Fig A1 in the Appendix.

Influence of injury metrics on helmet ranking

The helmeted impact condition affected brain strain peaks, but the effect was inconsistent among the five metrics (Fig 2B). In the seventeen helmets, strain peaks based on MPS, MTPN, and MTPS were significantly different ($p < 0.001$) in all three impact conditions, in which the ZRot induced the highest values, followed by YRot and XRot. For MTON, the ZRot remained as the condition with the highest value, while the YRot produced significantly smaller strain peaks than the XRot. When switching to MTOS, no significant difference ($p = 0.19$) was noted between XRot and YRot, while the ZRot instigated higher values than the other two impact conditions. The exact peaks based on the five strains for the 51 impact simulations are available in Fig 2C.

For the helmet ranking based on the strain peaks averaged among the three impact conditions, the same results were noted among the five strains for the high-ranked helmet, while significant disparities were noted in median-ranked and low-ranked helmets (Fig 2D). For example, Helmet Q was ranked the top (i.e., lowest strain), followed by Helmet D as the second and Helmet M as the third, independent of the strain type. For the low-ranked helmet, Helmet P was ranked lowest based on MPS, MTPN, MTOS, and MTPS, while Helmet N was ranked lowest based on MTON. We further quantified this ranking-related disparity using Kendall's tau (Fig 2E, below diagonal) with the coefficient value varying from 0.58 to 0.93. Only three Kendall's tau attained coefficient values over 0.8 (i.e., MPS vs. MTPN, MTON vs. MTOS, and MTPN vs. MTPS). For the interdependency among the five strains (Fig 2E, above diagonal), strong correlations (i.e., $r > 0.7$) were noted in all strain pairs, except for two cases (i.e., MTON vs. MTPS, MTOS vs. MTPS).

For the correlation between kinematic-based metrics and strain-based metrics (Fig 2F), all five strains

exhibited strong correlations (i.e., $r > 0.7$) with all five angular motion-related kinematic metrics, except for one case (i.e., PAA vs. MTPS). For the linear motion-related kinematics, all five strains were either insignificantly ($p > 0.05$) or moderately/weakly ($|r| < 0.6$) correlated with PLA and HIC.

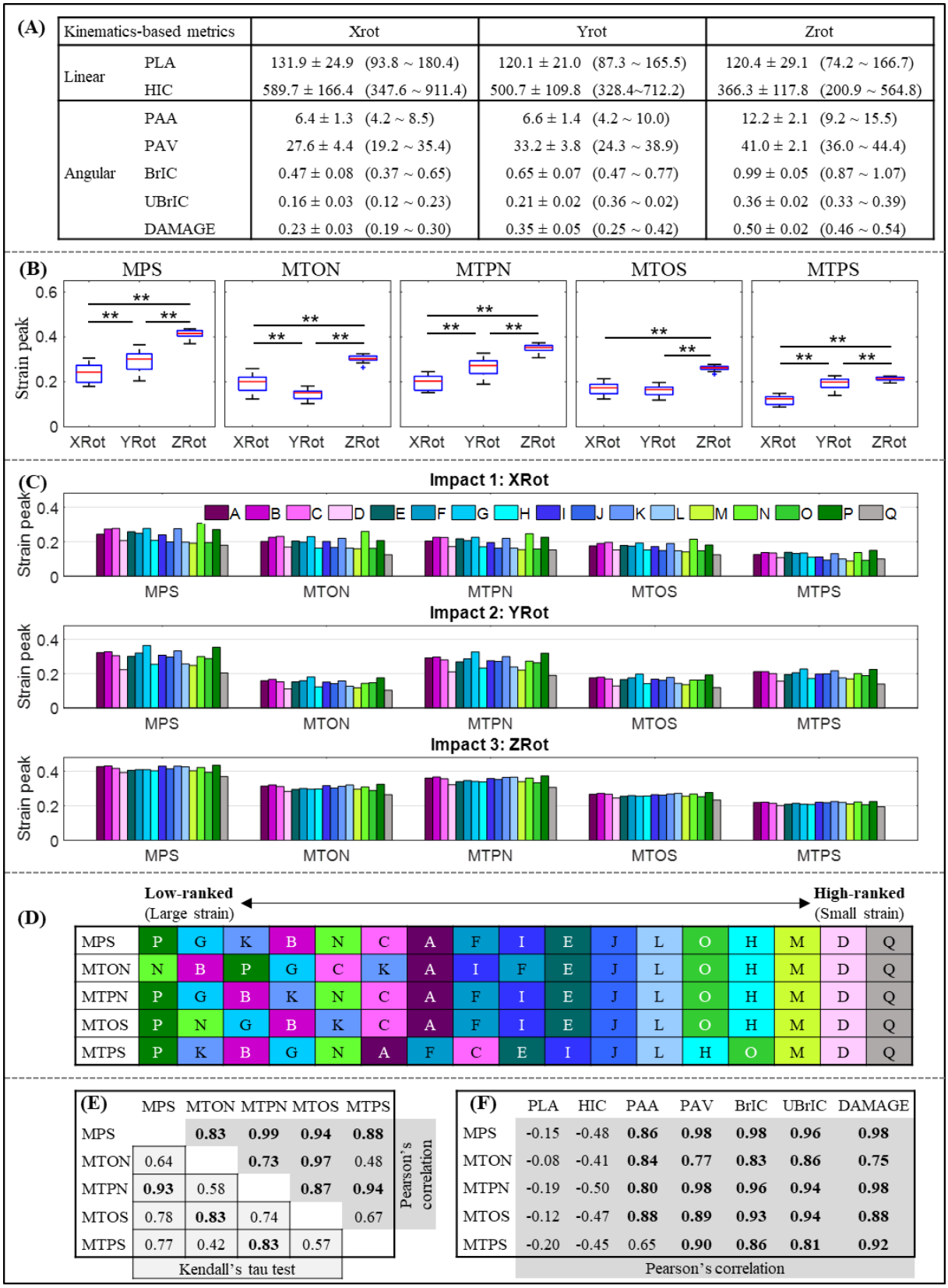

Fig. 2. (A) Summary of seven kinematic-based metrics in the form of mean ± standard deviation (range) for three

loading conditions (XRot, YRot, and ZRot). (B) Summary of five strain-based metrics in the form of boxplots for three loading conditions (XRot, YRot, and ZRot) (**p<0.001, Wilcoxon matched pairs signed rank test). (C) Strain peaks (95th percentile values) for three loading conditions in seventeen helmets (i.e., Helmets A-Q). (D) Ranking of seventeen helmets (Helmets A-Q) based on strain peaks (i.e., 95th percentile values averaged from three impact conditions based on five strain types). (E) Below diagonal (cells colored in light grey with border lines in black): Kendall's tau coefficient values to evaluate the sensitivity of helmet ranking on the choice of strain metrics with the coefficient values over 0.8 highlighted in bold. Above diagonal (cells in light gray with border lines unshown): Pearson's correlation coefficient value (r) between five strain-related metrics. The coefficient values over 0.7 (i.e., strong correlation) are highlighted in bold. (F) Pearson's correlation coefficient value (r) between five strain-related metrics and five kinematic-based metrics. The coefficient values over 0.7 (i.e., strong correlation) are highlighted in bold.

Brain strain distributions in helmeted impacts

To evaluate whether the helmet altered the strain pattern, we identified the elements with the strain value ranked within the top 5% of the given simulation (termed as high-strain elements) and plotted the results of three representative helmets, i.e., Helmet Q (high-ranked), Helmet E (medium-ranked), and Helmet P (low-ranked) (Fig 3A). It can be noted that the distribution of high-strain elements depended on the impact condition and strain type. Interestingly, the helmet type did not change the location of high-strain elements. Taking the MTON in YRot as an example, high-strain elements were consistently noted in the cerebral WM in the frontal and occipital lobes, and cerebellum WM for all three helmets. However, one exception was noted in XRot between Helmet Q and the other two helmets, regardless of the strain type. Using MTPN as an illustrative metric, high-strain elements were wholly located within the cerebral WM for Helmet Q, while partial high-strain elements were noted in cerebellum WM for Helmets E and P. While scrutinizing the normalized strain distribution (Fig 3B), we also noted similar results that under the same impact condition, the helmet type did not affect the normalized strain pattern with the only exception noted in XRot between Helmet Q and the other two helmets.

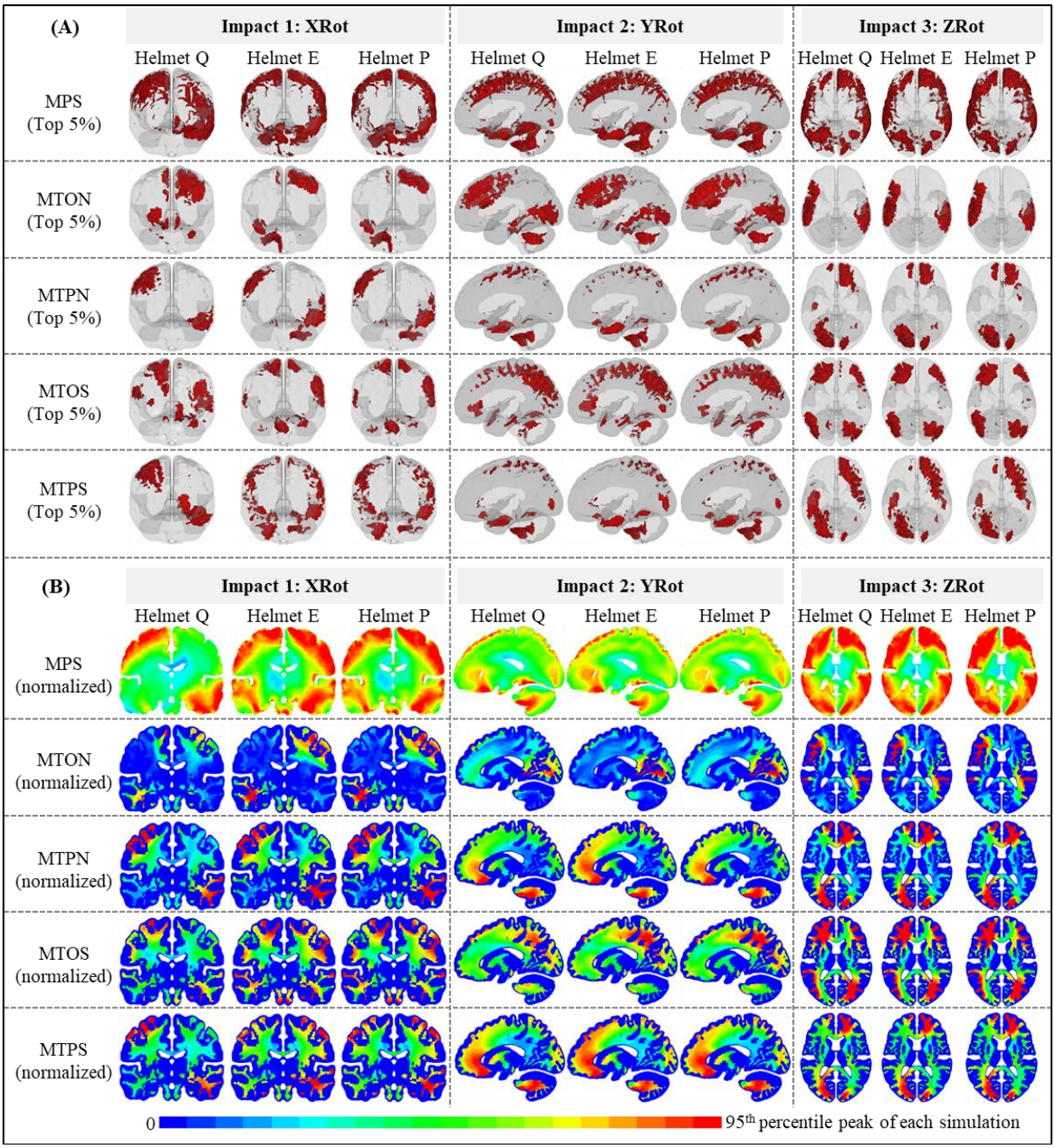

Fig. 3. Brain strain distribution in nine representative impacts (i.e., Helmets Q, E, and P in XRot, YRot, and ZRot). (**A**) Brain elements with the MPS values within the top 5% and white mater elements with the tract-related strain values within the top 5%. To facilitate the visualization, the pia mater is shown in transparent. (**B**) Normalized brain strain contours in coronal, sagittal, and horizontal views for XRot, YRot, and ZRot, respectively. Note that, as indicated by the upper limit of the legend bar, the strain in each contour was normalized by the 95th percentile strain values (available in Fig 2C) from the same simulation.

We further quantified the similarity in strain distribution by performing Pearson's correlation in element-wise strain peaks. Representative plots for the correlations between Helmet D and Helmet E in XRot were shown in Fig 4A with *r* values as 0.95 for MPS, 0.98 for MTON, 0.96 for MTPN, 0.95 for MTOS, and 0.92 for MTPS. We next extended the correlation to all seventeen helmets with the *r* value plotted in the form of heatmap in Fig 4B for XRot, Fig 4C for YRot, and Fig 4D for ZRot. Under a given impact condition, strong correlations ($r > 0.7$) in the element-wise strain results were noted in all seventeen helmets, regardless of the strain type. The only exception was noted between Helmet Q and

the other 16 helmets, in which only weak to moderate correlations ($r < 0.7$) were noted. Taken together, the correlation results of element-wise strain peaks quantitatively verified that the helmet did not change the strain pattern except for helmet Q in XRot.

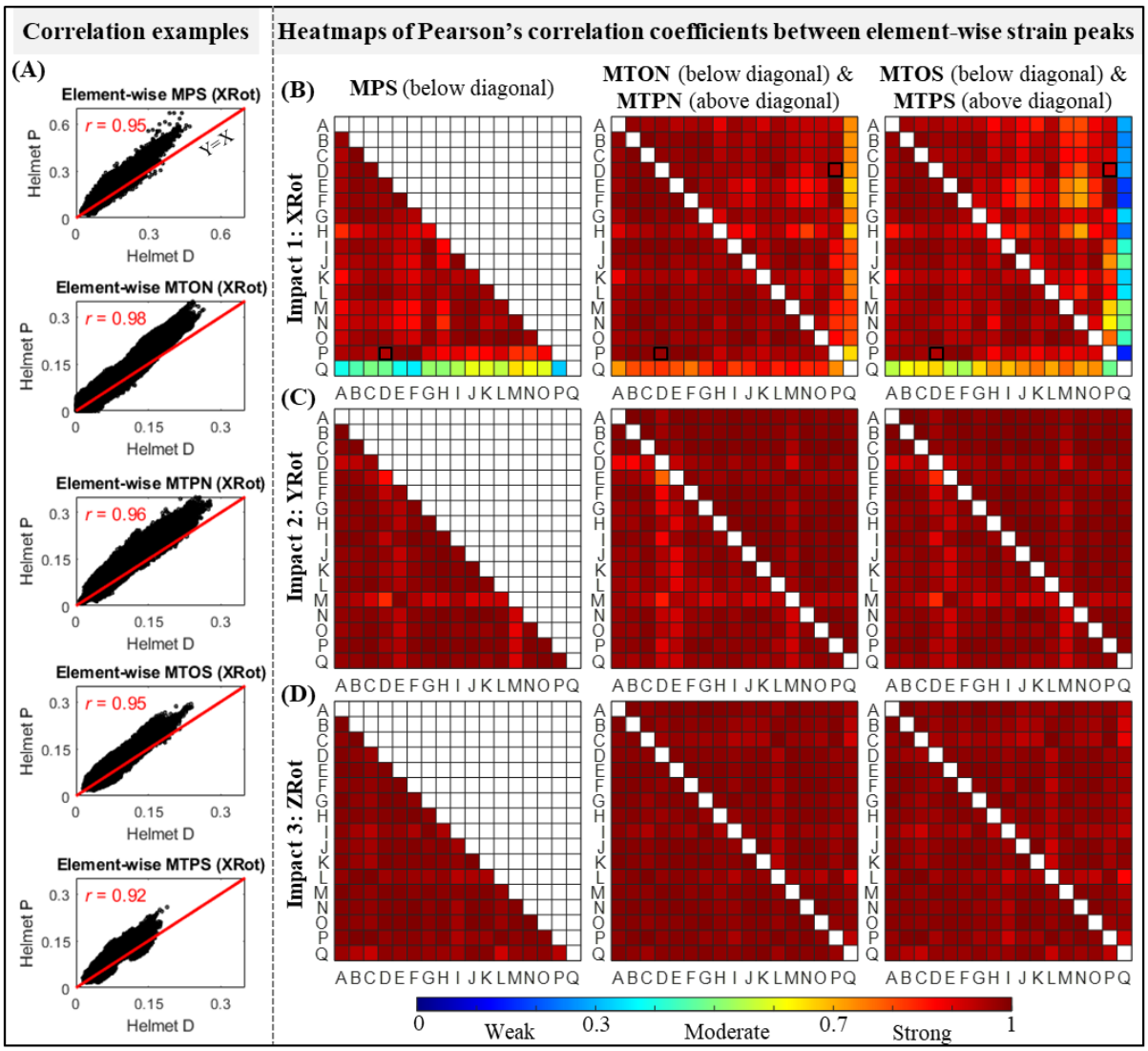

Fig. 4. Pearson's correlation coefficient (r) between element-wise MPS, MTON, MTPN, MTOS, and MTPS from 51 helmeted impacts (three impact scenarios, i.e., XRot, YRot, and ZRot, and 17 helmets, i.e., helmets A-Q). (**A**) Representative illustrations of Pearson's correlation for element-wise MPS, MTON, MTPN, MTOS, and MTPS from impact simulations with kinematics obtained from helmets D and P in XRot. (**B-D**) Heatmap of Pearson's correlation coefficient values for element-wise strain results between seventeen helmeted impacts under the condition of XRot, YRot and ZRot, respectively. Note that in subfigure B, the cells corresponding to the five specific correlations in subfigure A are highlighted with border lines in bold. In the legend, it was indicated that the coefficient value within the range of 0-0.3, 0.3-0.7, and 0.7-1 represented weak, moderate, and strong correlations, respectively.

Discussions

The current study investigated the peaks and distributions of five strain-based metrics in fifty-one helmeted impact simulations (seventeen helmets, three impact conditions). Our results showed both the helmet type and impact condition affected the strain peaks. The helmet ranking outcome based on the strain peaks was affected by the choice of injury metrics. Interestingly, under a given impact condition,

the helmet did not change the strain distribution with only one exception noted. This study reinforced the importance of mitigating the strain peaks in helmeted impacts and hinted at a possible new direction of helmet improvement by optimizing the strain distribution with accounting the selective vulnerability of different brain regions. Our work also provided new insight that the helmet ranking outcome was dependent on the choice of injury metrics.

Our results on the similarity of brain strain patterns under the same impact condition were generally agreed with the findings in previous *in vivo* imaging and computational studies. Knutsen *et al.* (2020) implemented tagged magnetic resonance imaging to measure MPS and MTON in twenty voluntary impacts with two head motions, i.e., ten neck rotations with primary angular motion within the axial plane and ten neck extensions with primary angular motion with the sagittal plane. It was found that strain patterns based on MPS and MTON were spatially consistent across volunteers for the same head motion. By excising one three-dimensional FE head model along the coronal plane by 44 synthetic angular velocity profiles with various shapes but the same PAV (23.4 rad/s) and duration (46.3 m/s), Zhao and Ji (2017) found that the MPS pattern remained largely consistent with the MPS peaks significantly changed. Similar findings were also reported by Carlsen *et al.* (2021) using three planar FE head models secondary to 100 idealized sinus-shaped angular loadings along the sagittal, coronal, and axial planes, respectively. Our study extended previous efforts by using realistic loadings recorded from seventeen bicycle helmets in three distinct impact conditions. These impact conditions represented the most common impact scenarios in bicycle accidents (Bourdet *et al.* 2012). Our results also further confirmed the early finding the strain peak was affected by the helmet type and impact condition. Relevant discussion on this has been extensively reported in the literature (Fahlstedt *et al.* 2014, Ito *et al.* 2014, Fahlstedt *et al.* 2016a, Fahlstedt *et al.* 2016b, Pipkorn *et al.* 2020, Abayazid *et al.* 2021, Hoshizaki *et al.* 2022, Lindgren *et al.* 2022, Rezayaraghi *et al.* 2023, Abayazid and Ghajari 2024, Li *et al.* 2024) and was not repeated here.

In our earlier study by Fahlstedt *et al.* (2021), eight independently developed FE head models were used to evaluate helmet performance. The current work significantly extended our earlier effort as well as the state-of-the-art from three different perspectives. Firstly, we utilized the ADAPT head model that uniquely featured with conforming meshes for the interface between the brain and cerebrospinal fluid, providing complementary and independent information to its eight counterparts used by Fahlstedt *et al.* (2021). Secondly, the majority of current literature employed MPS to evaluate helmets (Fahlstedt 2015, Emsley *et al.* 2024) with only three previous studies, to the best of the authors' knowledge, used MTON (Deck *et al.* 2017, Bradfield *et al.* 2018, Bliven *et al.* 2019). Thanks to the embedded fiber tracts in the ADAPT model, we were able to assess helmets by collectively examining the normal and shear strains along and perpendicular to the fiber tract as well as MPS (Fig 1D). Such an extensive examination has not been attempted before. Thirdly, we collectively monitored both the peak and distribution of full-field brain strain responses, while previous work primarily focused on the strain peaks. As both the

current work and the one by Fahlstedt *et al.* (2021) used the same helmet tests (Stigson *et al.* 2017), results from these two studies could be compared and integrated. When ranking the seventeen helmets, our study found the outcome was dependent on the choice of strain type (Kendall's tau coefficient: 0.58 ~ 0.93, Fig 2D-E). Comparable disparities were also presented by Fahlstedt *et al.* (2021) that eight FE head model ranked the helmet performance differently (Kendall's tau coefficient: 0.50 ~ 0.98, the exact helmet ranking outcomes are adapted from the original article and shown in Table 2). As no consensus has been reached on the best brain injury metric and discordant responses were noted among different FE head models, these two successive studies collectively highlighted that caution should be exercised when using computational models to rank helmet performance.

Table. 2. Ranking of 17 helmets using 8 different brain injury models (adapted from the study by Fahlstedt *et al.* (2021)).

Model	Metric	Low-ranked ←																→ High-ranked
GHBMC	MPS	P	K	G	N	B	C	A	I	F	E	J	L	O	H	M	D	Q
	CSDM	P	G	K	B	N	A	C	I	F	J	E	L	O	H	M	D	Q
IC	Strain	G	I	K	B	P	A	E	F	C	H	N	J	L	M	Q	O	D
	Strain rate	G	P	K	B	N	I	C	F	A	E	J	H	L	O	M	D	Q
KTH	MPS	P	G	K	B	N	C	F	I	A	E	J	O	L	H	M	Q	D
Piper	MPS	P	G	N	K	B	C	A	F	I	E	J	L	O	H	M	D	Q
SIMon	MPS	P	K	B	G	N	C	A	F	E	I	J	L	H	O	M	D	Q
	CSDM	P	K	N	G	B	C	A	F	I	E	J	L	O	H	M	D	Q
THUMS	MPS	P	K	N	B	G	A	C	I	F	J	E	L	O	H	M	D	Q
UCDBTM	MPS	G	B	I	P	D	K	E	F	C	H	N	A	M	J	Q	L	O
WHIM	MPS	P	G	K	B	N	C	A	F	I	E	J	L	O	H	M	D	Q

Our study provided important implications for helmet improvement. The large variations in MPS at the whole brain level and tract-related strain peaks at the whole WM level (Fig 2B-C) implied that existing helmets could still be improved by mitigating the strain peak, as has been reported before (Fahlstedt *et al.* 2016a, Deck *et al.* 2019, Abayazid *et al.* 2021, Hoshizaki *et al.* 2022, Lindgren *et al.* 2022, Li *et al.* 2024). This implication was based on the rationale that the peak strain represented the worst scenario and was most likely to cause injury. However, it did not recognize that different brain regions responded differently to identical mechanical stimuli. For example, Morrison III and colleagues stretched *in vitro* cultured hippocampal and cortical tissues from rats and found, compared to the cortex, the hippocampus was more susceptible to injury in the form of cell death (Cater *et al.* 2006, Elkin and Morrison III 2007) and electrophysiological impairment (Kang and Morrison III 2015a, b). In light of this, we studied the brain strain distribution in fifty-one helmeted impacts, qualitatively (Fig 3) and quantitatively (Fig 4), with the involvement of all brain elements for MPS and all WM elements for four tract-related strain peaks. Our results found evident similarity in strain patterns in all seventeen helmets (with only one exception that is discussed later), indicating that different helmets did not change the path of mechanical force transmission within the brain during impacts (Carlsen *et al.* 2021). Such results hinted that the protective performance of existing helmets could be further augmented by optimizing strain distribution by accounting the selective vulnerability of brain subregions, i.e., redistributing the

brain strain with a relatively large dose in the region that was more resistant to injury and a relatively small dose in the region that was more prone to injury. It should be clarified that such an improvement is at the conceptual stage as the exact values of region-specific injury criteria for the human brain are largely elusive today. Initial attempts have been noted to use human FE head models to derive region-specific injury risk functions (Zhang *et al.* 2004, Kleiven 2007, Giordano and Kleiven 2014, Sahoo *et al.* 2016, Zhao *et al.* 2017, Wu *et al.* 2020, Wu *et al.* 2021, Zhou *et al.* 2021, Fahlstedt *et al.* 2022, Wu *et al.* 2022). For example, early studies proposed the thresholds of 50% risk of concussion to be 0.26 for gray matter and 0.21 for corpus callosum based on MPS (Kleiven 2007), and 0.15 for brainstem and 0.07 for corpus callosum based on MTON (Giordano and Kleiven 2014). However, these risk functions were derived by correlating continuous strain-based metrics to binary-diagnosed injury outcomes (concussion or no-concussion), where definitive pathologies at specific regions were lacking. Thereby, further evaluation was needed to assess the reliability of these aforementioned region-specific risk functions derived from human FE head models.

The lack of similarity in strain patterns between Helmet Q and the other sixteen helmets in XRot could be explained by the disparity in impact kinematics. As shown in Fig A1 in the Appendix, Helmet Q had comparable angular motion in all three anatomical directions with the peak angular velocity as -11.7, -12.7, and -9.6 rad/s for X-, Y- and Z-axes, respectively. This was distinctly different from the pattern of directional angular velocity peaks noted from the other sixteen helmets, in which primary rotation motion was noted within the coronal plane (e.g., -24.4 rad/s along the X-axis, -6.9 rad/s along the Y-axis, and -4.7 rad/s along the Z-axis for Helmet P). We speculated that the peculiar loading profile measured from Helmet Q in XRot might be related to the geometry or design of this specific helmet (e.g., this helmet was tested with an additional cover). We acknowledged the exact reason responsible for the discordant results remained unknown. To facilitate a direct comparison with the study by Fahlstedt *et al.* (2021) we decided to retain Helmet Q in the current study.

For the correlation between kinematic-based metrics and strain-based metrics, we found the tract-related strains (i.e., MTON, MTPN, MTOS, MTPS) strongly correlated ($r > 0.7$) with angular motion-based metrics (e.g., PAV and PAA) (Fig 2F). To the best of our knowledge, only one imaging study reported all four tract-related strains significantly ($p < 0.05$) correlated with both PAV and PAA during voluntary impacts (Zhou *et al.* 2024). In addition, a few computational studies (Hajiaghamemar *et al.* 2020a, Wu *et al.* 2020, Carlsen *et al.* 2021) reported that MTON correlated with PAV at short-duration impacts and with PAA at long-duration impacts, of which the head impact severity was within or close to the traumatic level. Taken together, these studies highlighted that the axonal fiber deformation was primarily instigated by angular motion, instead of linear motion. However, it should also be noted that no agreement was reached among the four tract-related strains regarding the angular motion-based metric with the highest coefficient value. This might be related to the fundamental differences of these four strains (normal and shear strain oriented along and perpendicular to the fiber tract, respectively)

and relatively limited loading samples (51 helmeted impacts) in our study. Our study also found that the MPS derived from the ADAPT model correlated well with angular motion-related metrics, but not with two linear motion-related metrics (i.e., PLA, HIC) (Fig 2F). Similar correlations have also been noted based on the MPS extracted from the other eight FE models evaluated by Fahlstedt *et al.* (2021).

Although the current study yielded some new insight into the brain strain dynamics in helmeted impacts, several caveats should be noted. First, we only involved seventeen bicycle helmets, representing a relatively small sample size than some other studies, e.g., 27 bicycle helmets by Abayazid *et al.* (2021), 30 bicycle helmets by Bland *et al.* (2020), 35 bicycle helmets by Deck *et al.* (2019). The current study could be extended by involving more bicycle helmets and even other helmet types, e.g., motorcycle helmets (Yu *et al.* 2022), ice hockey helmets (Rowson *et al.* 2015), and football helmets (Rowson and Duma 2011), etc. Second, the responses of the ADAPT model have been previously evaluated by experimental data of brain MPS and maximum principal strain rate, brain-skull relative motion and intracranial pressure (Li *et al.* 2021, Zhou *et al.* 2023) and showed good correlation with the brain injury pattern in a skiing accident (based on MPS) (Yuan *et al.* 2024) and a concussive impact in American football (based on MTON) (Montanino *et al.* 2021). In the current study, we used the ADAPT model to predict brain responses in helmeted impacts based on MPS and four other tract-related strains. As aforementioned, only one *in vivo* imaging study (Zhou *et al.* 2024) calculated all four types of tract-related strains with impact severity far from the loading regime in our work. Thereby, the accuracy of FE-derived tract-related strains remained to be further evaluated by their experimental counterparts measured from impact severity close to injury. However, it should be noted that this limitation was not necessarily specific to our study and instead represented significant challenges in the research field of brain injury biomechanics. Lastly, our work was based on the early conducted bicycle helmet tests where relevant limitations have been exhaustively discussed elsewhere (Stigson *et al.* 2017, Fahlstedt *et al.* 2021) and not repeated here.

Conclusion

This study investigated brain strain distributions and peaks in fifty-one helmeted impacts, encompassing seventeen commonly used bicycle helmets and three critical impact conditions. We found that the strain distribution depended on the impact condition but not on the helmet type, while the strain peak was significantly influenced by both. The helmet ranking outcome based on the strain peaks was affected by the choice of injury metrics. It was also shown that angular motion-related metrics significantly correlated with tract-related strains in the WM and MPS in the brain. Our study provided new insights into the computational brain biomechanics and helmet evaluation using tissue-based strain peaks. Our results hinted that the protective performance of helmets could be augmented by mitigating the strain peak and optimizing the strain distribution by accounting the selective vulnerability of brain subregions.

Acknowledgments

This research has received funding from KTH Royal Institute of Technology (Stockholm, Sweden), the Swedish Governmental Agency for Innovation systems (VINNOVA) (no. 2023-00753), and private funds from Mips AB. The content of this article is solely the responsibility of the authors and does not necessarily represent the official views of neither funding agencies. The authors also acknowledge Folksam, Sweden for sharing the bicycle helmet test results. The computational simulations were enabled by resources provided by the National Academic Infrastructure for Supercomputing in Sweden (NAISS) at the center for High Performance Computing (PDC) partially funded by the Swedish Research Council through grant agreement no. 2022-06725.

Conflict of Interest

MF was employed by Mips AB. Authors ZZ, XL and SK received contracted private funds from Mips AB that supported the work. However, this does not construct as a potential conflict of interest.

References

Abayazid, F., Ding, K., Zimmerman, K., Stigson, H., Ghajari, M., 2021. A new assessment of bicycle helmets: The brain injury mitigation effects of new technologies in oblique impacts. Annals of biomedical engineering 49 (10), 2716-2733.
Abayazid, F.F., Ghajari, M., 2024. Viscoelastic circular cell honeycomb helmet liners for reducing head rotation and brain strain in oblique impacts. Materials & Design, 112748.
Baker, C.E., Yu, X., Patel, S., Ghajari, M., 2023. A review of cyclist head injury, impact characteristics and the implications for helmet assessment methods. Annals of biomedical engineering 51 (5), 875-904.
Bandak, F., Eppinger, R.H., Year. Three-dimensional finite element analysis of the human brain under combined rotational and translational accelerations. In: Proceedings of the Proceedings: Stapp Car Crash Conference, pp. 145-163.
Bland, M.L., Mcnally, C., Zuby, D.S., Mueller, B.C., Rowson, S., 2020. Development of the star evaluation system for assessing bicycle helmet protective performance. Annals of biomedical engineering 48, 47-57.
Bliven, E., Rouhier, A., Tsai, S., Willinger, R., Bourdet, N., Deck, C., Madey, S., Bottlang, M., 2019. A novel strategy for mitigation of oblique impacts in bicycle helmets. J. Forensic Biomed 10 (8).
Bourdet, N., Deck, C., Carreira, R.P., Willinger, R., 2012. Head impact conditions in the case of cyclist falls. Proceedings of the Institution of Mechanical Engineers, Part P: Journal of sports engineering and technology 226 (3-4), 282-289.
Bradfield, C., Vavalle, N., Devincentis, B., Wong, E., Luong, Q., Voo, L., Carneal, C., 2018. Combat helmet suspension system stiffness influences linear head acceleration and white matter tissue strains: Implications for future helmet design. Military medicine 183 (suppl_1), 276-286.
Carlsen, R.W., Fawzi, A.L., Wan, Y., Kesari, H., Franck, C., 2021. A quantitative relationship between rotational head kinematics and brain tissue strain from a 2-d parametric finite element analysis. Brain Multiphysics 2, 100024.
Cater, H.L., Sundstrom, L.E., Morrison Iii, B., 2006. Temporal development of hippocampal cell death is dependent on tissue strain but not strain rate. Journal of biomechanics 39 (15), 2810-2818.
Dau, N., Hansen, K., Madey, S., Bottlang, M., 2012. Bicycle helmet impact test method designed to induce rotational acceleration. Legacy Biomechanics Lab, Legacy Research and Development Center, Portland, OR www. biomechresearch. org.

Deck, C., Bourdet, N., Halldin, P., Debruyne, G., Willinger, R., Year. Protection capability of bicycle helmets under oblique impact assessed with two separate brain fe models. In: Proceedings of the IRCOBI Conference Proceedings.
Deck, C., Bourdet, N., Meyer, F., Willinger, R., 2019. Protection performance of bicycle helmets. Journal of safety research 71, 67-77.
Elkin, B.S., Morrison Iii, B., 2007. Region-specific tolerance criteria for the living brain. Stapp car crash journal 51, 127-138.
Emsley, B., Farmer, J., Sherratt, P., Goodall, P., Jackson, T., West, A., 2024. An overview of the test methodology used in current cycling helmet standards and literature. International Journal of Impact Engineering, 104928.
Fahlstedt, M., 2015. Numerical accident reconstructions: A biomechanical tool to understand and prevent head injuries. KTH Royal Institute of Technology.
Fahlstedt, M., Abayazid, F., Panzer, M.B., Trotta, A., Zhao, W., Ghajari, M., Gilchrist, M.D., Ji, S., Kleiven, S., Li, X., 2021. Ranking and rating bicycle helmet safety performance in oblique impacts using eight different brain injury models. Annals of biomedical engineering 49, 1097-1109.
Fahlstedt, M., Halldin, P., Kleiven, S., Year. Importance of the bicycle helmet design and material for the outcome in bicycle accidents. In: Proceedings of the International Cycling Safety Conference, November 18-19, 2014, Gothenburg, Sweden, pp. 1-14.
Fahlstedt, M., Halldin, P., Kleiven, S., 2016a. The protective effect of a helmet in three bicycle accidents—a finite element study. Accident Analysis & Prevention 91, 135-143.
Fahlstedt, M., Halldin, P., S Alvarez, V., Kleiven, S., Year. Influence of the body and neck on head kinematics and brain injury risk in bicycle accident situations. In: Proceedings of the IRCOBI 2016, pp. 459-478.
Fahlstedt, M., Meng, S., Kleiven, S., 2022. Influence of strain post-processing on brain injury prediction. Journal of Biomechanics 132, 110940.
Gabler, L.F., Crandall, J.R., Panzer, M.B., 2018. Development of a metric for predicting brain strain responses using head kinematics. Annals of biomedical engineering 46, 972-985.
Gabler, L.F., Crandall, J.R., Panzer, M.B., 2019. Development of a second-order system for rapid estimation of maximum brain strain. Annals of biomedical engineering 47, 1971-1981.
Giordano, C., Kleiven, S., 2014. Evaluation of axonal strain as a predictor for mild traumatic brain injuries using finite element modeling. Stapp car Crash Journal 58, 29-61.
Hajiaghamemar, M., Seidi, M., Margulies, S.S., 2020a. Head rotational kinematics, tissue deformations, and their relationships to the acute traumatic axonal injury. Journal of biomechanical engineering 142 (3), 031006.
Hajiaghamemar, M., Wu, T., Panzer, M.B., Margulies, S.S., 2020b. Embedded axonal fiber tracts improve finite element model predictions of traumatic brain injury. Biomechanics and modeling in mechanobiology 19, 1109-1130.
Halldin, P., Aare, M., Kleiven, S., Von Holst, H., Year. Improved helmet design and test methods to reduce rotational induced brain injuries. In: Proceedings of the RTO specialist meeting, the NATO's research and Technology organization (RTO).
Halldin, P., Gilchrist, A., Mills, N., 2001. A new oblique impact test for motorcycle helmets. International Journal of Crashworthiness 6 (1), 53-64.
Hansen, K., Dau, N., Feist, F., Deck, C., Willinger, R., Madey, S.M., Bottlang, M., 2013. Angular impact mitigation system for bicycle helmets to reduce head acceleration and risk of traumatic brain injury. Accident Analysis & Prevention 59, 109-117.
Hoshizaki, T., Post, A.M., Zerpa, C.E., Legace, E., Hoshizaki, T.B., Gilchrist, M.D., 2022. Evaluation of two rotational helmet technologies to decrease peak rotational acceleration in cycling helmets. Scientific reports 12 (1), 7735.
Ito, D., Yamada, H., Oida, K., Mizuno, K., Year. Finite element analysis of kinematic behavior of cyclist and performance of cyclist helmet for human head injury in vehicle-to-cyclist collision. In: Proceedings of the IRCOBI Conference. International Research Council on Biomechanics of Injury, pp. 119-131.
Johnson, V.E., Stewart, W., Smith, D.H., 2013. Axonal pathology in traumatic brain injury. Experimental neurology 246, 35-43.

Kang, W.H., Morrison Iii, B., 2015a. Functional tolerance to mechanical deformation developed from organotypic hippocampal slice cultures. Biomechanics and modeling in mechanobiology 14 (3), 561-575.
Kang, W.H., Morrison Iii, B., 2015b. Predicting changes in cortical electrophysiological function after in vitro traumatic brain injury. Biomechanics and modeling in mechanobiology 14 (5), 1033-1044.
King, A.I., Yang, K.H., Zhang, L., Hardy, W., Viano, D.C., Year. Is head injury caused by linear or angular acceleration. In: Proceedings of the International Research Council on Biomechanics of Injury, Lisbon, Portugal.
Kleiven, S., 2006. Evaluation of head injury criteria using a finite element model validated against experiments on localized brain motion, intracerebral acceleration, and intracranial pressure. International Journal of Crashworthiness 11 (1), 65-79.
Kleiven, S., 2007. Predictors for traumatic brain injuries evaluated through accident reconstructions. Stapp car Crash Journal 51, 81-114.
Kleiven, S., 2013. Why most traumatic brain injuries are not caused by linear acceleration but skull fractures are. Frontiers in bioengineering and biotechnology 1, 15.
Klug, C., Feist, F., Tomasch, E., 2015. Testing of bicycle helmets for preadolescents. International Research Council on the Biomechanics of Injury (IRCOBI), Lyon, France, 136-155.
Knutsen, A.K., Gomez, A.D., Gangolli, M., Wang, W.-T., Chan, D., Lu, Y.-C., Christoforou, E., Prince, J.L., Bayly, P.V., Butman, J.A., 2020. In vivo estimates of axonal stretch and 3d brain deformation during mild head impact. Brain multiphysics 1, 100015.
Leng, B., Ruan, D., Tse, K.M., 2022. Recent bicycle helmet designs and directions for future research: A comprehensive review from material and structural mechanics aspects. International Journal of Impact Engineering 168, 104317.
Li, X., Von Schantz, A., Fahlstedt, M., Halldin, P., 2024. Evaluating child helmet protection and testing standards: A study using piper child head models aged 1.5, 3, 6, and 18 years. PLoS one 19 (1), e0286827.
Li, X., Zhou, Z., Kleiven, S., 2021. An anatomically detailed and personalizable head injury model: Significance of brain and white matter tract morphological variability on strain. Biomechanics and modeling in mechanobiology 20, 403-431.
Lindgren, N., Halldin, P., Fahlstedt, M., Year. Influence of headform on assessments and ratings of the protective performance of bicycle helmets. In: Proceedings of the International Research Council on the Biomechanics of Injury, porto, Portugal, pp. 892-911.
Meng, S., Ivarsson, P., Lubbe, N., 2023. Evaluation of full-face, open-face, and airbag-equipped helmets for facial impact protection. Accident Analysis & Prevention 191, 107181.
Mills, N., Gilchrist, A., 2008. Oblique impact testing of bicycle helmets. International Journal of Impact Engineering 35 (9), 1075-1086.
Montanino, A., Li, X., Zhou, Z., Zeineh, M., Camarillo, D., Kleiven, S., 2021. Subject-specific multiscale analysis of concussion: From macroscopic loads to molecular-level damage. Brain multiphysics 2, 100027.
Næss, I., Galteland, P., Skaga, N.O., Eken, T., Helseth, E., Ramm-Pettersen, J., 2020. The number of patients hospitalized with bicycle injuries is increasing-a cry for better road safety. Accident Analysis & Prevention 148, 105836.
Piatkowski, D., Bopp, M., 2021. Increasing bicycling for transportation: A systematic review of the literature. Journal of Urban Planning and Development 147 (2), 04021019.
Pipkorn, B., Alvarez, V., Fahlstedt, M., Lundin, L., Year. Head injury risks and countermeasures for a bicyclist impacted by a passenger vehicle. In: Proceedings of the Proceedings of IRCOBI Conference.
Ratner, B., 2009. The correlation coefficient: Its values range between+ 1/− 1, or do they? Journal of targeting, measurement and analysis for marketing 17 (2), 139-142.
Rezayaraghi, F., Abderezaei, J., Ozkaya, E., Stein, D., Pionteck, A., Kurt, M., 2023. Modal analysis of computational human brain dynamics during helmeted impacts. Brain Multiphysics 5, 100082.
Rizzi, M., Stigson, H., Krafft, M., Year. Cyclist injuries leading to permanent medical impairment in sweden and the effect of bicycle helmets. In: Proceedings of the Ircobi Conference, pp. 11-13.
Rowson, B., Rowson, S., Duma, S.M., 2015. Hockey star: A methodology for assessing the biomechanical performance of hockey helmets. Annals of biomedical engineering 43, 2429-2443.

Rowson, S., Duma, S.M., 2011. Development of the star evaluation system for football helmets: Integrating player head impact exposure and risk of concussion. Annals of biomedical engineering 39, 2130-2140.
Sahoo, D., Deck, C., Willinger, R., 2016. Brain injury tolerance limit based on computation of axonal strain. Accident Analysis & Prevention 92, 53-70.
Sarmiento, K., 2021. Emergency department visits for bicycle-related traumatic brain injuries among children and adults—united states, 2009–2018. MMWR. Morbidity and mortality weekly report 70.
Scholten, A.C., Polinder, S., Panneman, M.J., Van Beeck, E.F., Haagsma, J.A., 2015. Incidence and costs of bicycle-related traumatic brain injuries in the netherlands. Accident Analysis & Prevention 81, 51-60.
Song, H., Mcewan, P.P., Ameen-Ali, K.E., Tomasevich, A., Kennedy-Dietrich, C., Palma, A., Arroyo, E.J., Dolle, J.-P., Johnson, V.E., Stewart, W., Smith, D.H., 2022. Concussion leads to widespread axonal sodium channel loss and disruption of the node of ranvier. Acta Neuropathologica 144 (5), 967-985.
Stigson, H., Rizzi, M., Ydenius, A., Engström, E., Kullgren, A., Year. Consumer testing of bicycle helmets. In: Proceedings of the Proceedings of the IRCOBI Conference. Antwerp, Belgium, pp. 173-181.
Takhounts, E.G., Craig, M.J., Moorhouse, K., Mcfadden, J., Hasija, V., 2013. Development of brain injury criteria (bric). Stapp car crash journal 57, 243-266.
Versace, J., Year. A review of the severity index. In: Proceedings of the Proceeding of the 15th Stapp Car Crash Conference, 1972, Coronado, pp. 771-796.
Wang, F., Peng, K., Zou, T., Li, Q., Li, F., Wang, X., Wang, J., Zhou, Z., 2023. Numerical reconstruction of cyclist impact accidents: Can helmets protect the head-neck of cyclists? Biomimetics 8 (6), 456.
Whyte, T., Stuart, C., Mallory, A., Ghajari, M., Plant, D., Siegmund, G.P., Cripton, P.A., 2019. A review of impact testing methods for headgear in sports: Considerations for improved prevention of head injury through research and standards. Journal of biomechanical engineering 141 (7), 070803.
Willinger, R., Deck, C., Halldin, P., Otte, D., Year. Towards advanced bicycle helmet test methods. In: Proceedings of the International Cycling Safety Conference, pp. 18-19.
Wu, T., Antona-Makoshi, J., Alshareef, A., Giudice, J.S., Panzer, M.B., 2020. Investigation of cross-species scaling methods for traumatic brain injury using finite element analysis. Journal of neurotrauma 37 (2), 410-422.
Wu, T., Hajiaghamemar, M., Giudice, J.S., Alshareef, A., Margulies, S.S., Panzer, M.B., 2021. Evaluation of tissue-level brain injury metrics using species-specific simulations. Journal of neurotrauma 38 (13), 1879-1888.
Wu, T., Sato, F., Antona-Makoshi, J., Gabler, L.F., Giudice, J.S., Alshareef, A., Yaguchi, M., Masuda, M., Margulies, S.S., Panzer, M.B., 2022. Integrating human and nonhuman primate data to estimate human tolerances for traumatic brain injury. Journal of biomechanical engineering 144 (7), 071003.
Yu, X., Logan, I., De Pedro Sarasola, I., Dasaratha, A., Ghajari, M., 2022. The protective performance of modern motorcycle helmets under oblique impacts. Annals of biomedical engineering 50 (11), 1674-1688.
Yuan, Q., Li, X., Zhou, Z., Kleiven, S., 2024. A novel framework for video-informed reconstructions of sports accidents: A case study correlating brain injury pattern from multimodal neuroimaging with finite element analysis. Brain Multiphysics 6, 100085.
Zhang, L., Yang, K.H., King, A.I., 2004. A proposed injury threshold for mild traumatic brain injury. J. Biomech. Eng. 126 (2), 226-236.
Zhao, W., Cai, Y., Li, Z., Ji, S., 2017. Injury prediction and vulnerability assessment using strain and susceptibility measures of the deep white matter. Biomechanics and modeling in mechanobiology 16, 1709-1727.
Zhao, W., Ji, S., 2017. Brain strain uncertainty due to shape variation in and simplification of head angular velocity profiles. Biomechanics and modeling in mechanobiology 16, 449-461.
Zhou, Z., Christoffer, O., T. Christian, G., Xiaogai, L., Svein, K., 2024. In vivo white matter tract-related deformation during volunteer impacts. BioRxiv.
Zhou, Z., Li, X., Liu, Y., Fahlstedt, M., Georgiadis, M., Zhan, X., Raymond, S.J., Grant, G., Kleiven, S., Camarillo, D., 2021. Toward a comprehensive delineation of white matter tract-related deformation. Journal of neurotrauma 38 (23), 3260-3278.

Zhou, Z., Li, X., Liu, Y., Hardy, W.N., Kleiven, S., 2023. Brain strain rate response: Addressing computational ambiguity and experimental data for model validation. Brain Multiphysics 4, 100073.
Zhou, Z., Wang, T., Jörgens, D., Li, X., 2022. Fiber orientation downsampling compromises the computation of white matter tract-related deformation. journal of the mechanical behavior of biomedical materials 132, 105294.

Appendix

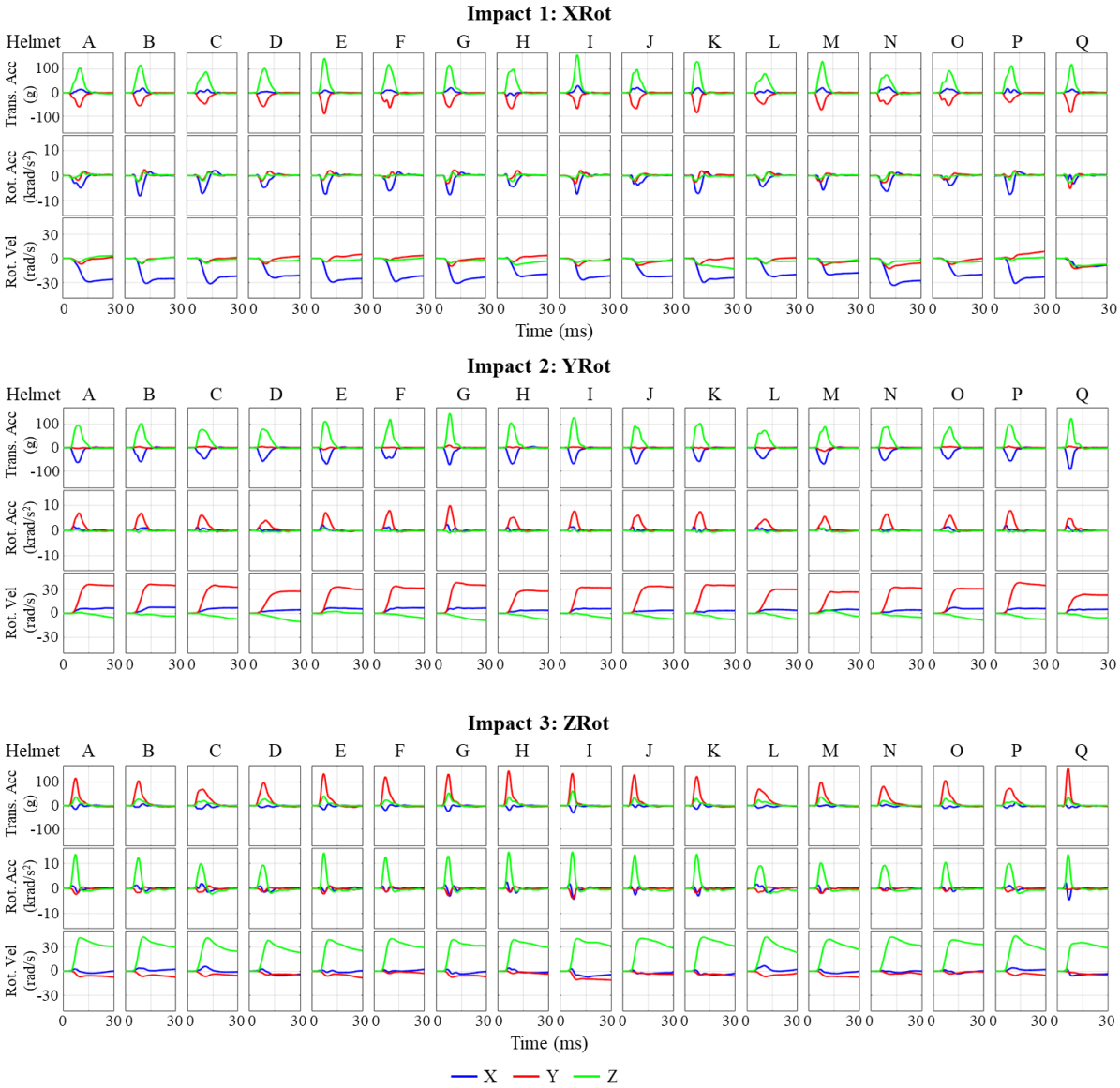

Fig. A1. Experimental kinematics under impact 1 (i.e., XRot), impact 2 (i.e., YRot), and impact 3 (i.e., ZRot) measured from 17 helmets. The anatomical coordinate systems (i.e., XYZ in the legend) that experimental kinematics expressed with are the one in Fig 1B.